

# Large magnetoresistance in LaBi: origin of field-induced resistivity upturn and plateau in compensated semimetals

Shanshan Sun<sup>1,†</sup>, Qi Wang<sup>1,†</sup>, Peng-Jie Guo<sup>1,†</sup>, Kai Liu<sup>1</sup>, and Hechang Lei<sup>1,\*</sup>

<sup>1</sup>Department of Physics and Beijing Key Laboratory of Opto-electronic Functional Materials & Micro-nano Devices, Renmin University of China, Beijing 100872, China

E-mail: hlei@ruc.edu.cn

**Abstract.** The discovery of non-magnetic extreme magnetoresistance (XMR) materials has induced great interests because the XMR phenomenon challenges our understanding of how a magnetic field can alter electron transport in semimetals. Among XMR materials, the LaSb shows XMR and field-induced exotic behaviors but it seems to lack the essentials for these properties. Here, we study the magnetotransport properties and electronic structure of LaBi, isostructural to LaSb. LaBi exhibits large MR as in LaSb, which can be ascribed to the nearly compensated electron and hole with rather high mobilities. More importantly, our analysis suggests that the XMR as well as field-induced resistivity upturn and plateau observed in LaSb and LaBi can be well explained by the two-band model with the compensation situation. We present the critical conditions leading to these field-induced properties. It will contribute to understanding the XMR phenomenon and explore novel XMR materials.

PACS numbers: 72.15.-v, 72.15.Gd, 71.30.+h, 71.20.Eh

## 1. Introduction

Magnetoresistance (MR) is the change of electronic resistance with magnetic field. It is not only one of most important topics in condensed matter physics but also vital to practical applications, such as magnetic field sensors, read heads of hard drives, random access memories [1]. In general, the large MR is emergent in magnetic materials, such as giant MR (GMR,  $\text{MR} \sim 10^2 \%$ ) in metallic thin films and colossal MR (CMR,  $\text{MR} \sim 10^4 \%$ ) in Cr-based chalcogenide spinels as well as Mn-based perovskites [2, 3, 4]. In the past several years, a series of non-magnetic metals with extreme MR (XMR) have been discovered, such as  $TPn$  ( $T = \text{Nb}$  and  $\text{Ta}$ ,  $Pn = \text{P}$  and  $\text{As}$ ) [5, 6, 7],  $\text{Cd}_3\text{As}_2$  [8],  $\text{NbSb}_2$  [9] and  $\text{WTe}_2$  [10]. These discoveries greatly challenge the traditional understanding that the non-magnetic metals usually have a small MR of only about a few percent. Most of novel XMR materials exhibit some common features, such as extremely high mobilities  $\mu$ , usually  $\mu > 1 \times 10^4 \text{ cm}^2 \text{ V}^{-1} \text{ s}^{-1}$ , and comparable carrier concentrations of electron and hole [5, 6, 7, 8, 10]. Based on these features, several mechanisms have been proposed to explain the origin of XMR in these materials, including topological protection from backscattering mechanism in Dirac and Weyl semimetals (SMs) [7, 8], and electron-hole compensation mechanism [10].

Very recently, the XMR materials are extended to the rare-earth-based material  $\text{LaSb}$  with simple rock-salt structure [11]. It shows XMR at 2 K and 9 T ( $0.9 \times 10^6 \%$ ). Moreover, metallic  $\text{LaSb}$  exhibits the field-induced upturn behavior in resistivity curve appearing at low temperature, followed by a resistivity plateau. Similar phenomena are also observed in several systems, such as  $\text{NbP}$  and  $\text{WTe}_2$  [6, 10]. Although the XMR in  $\text{LaSb}$  and  $\text{LaBi}$  have been reported in early works [12, 13], the origin of field-induced upturn behavior and resistivity plateau is not clear. Previous study [11] suggests that the prerequisites for XMR and related field-induced properties seem absent in  $\text{LaSb}$ , such as the inversion symmetry broken as in Weyl SMs, linear dispersion of band structure near Fermi energy level  $E_F$  as in Dirac SMs, and perfect electron-hole compensation satisfying the resonance situation as in  $\text{WTe}_2$ . Tafti et al proposed that the conducting surface states of a topological insulator protected by time reversal symmetry could be the reason causing these field-induced behaviors in  $\text{LaSb}$  [11]. But recent angle-resolved photoemission spectroscopy (ARPES) measurement suggests that  $\text{LaSb}$  is topologically trivial, no Dirac-like surface states are observed [14]. Moreover, the ARPES results also indicate that the carriers in  $\text{LaSb}$  are almost compensated. Thus, it is interesting to study whether electron-hole compensation mechanism is valid to explain these exotic phenomena in  $\text{LaSb}$ .

In order to explore more XMR materials in this family and understand field-induced properties in  $\text{LaSb}$  as well as other XMR materials, here, we report the detailed study on magnetotransport properties and electronic structure of  $\text{LaBi}$  single crystals, isostructural to  $\text{LaSb}$ . We find  $\text{LaBi}$  exhibits the XMR behavior, consistent with previous results [13]. Furthermore, the field-induced resistivity upturn and plateau shown in  $\text{LaSb}$  are also observed in  $\text{LaBi}$ . Importantly, the XMR and field-induced

phenomena in  $\text{LaPn}$  can be well understood in the framework of the classical multi-band model. Based on this simple model, we present the key conditions leading to these field-induced behaviors.

## 2. Experimental

Single crystals of  $\text{LaBi}$  were grown by the In flux. The elements were put into alumina crucible and sealed in quartz ampoule under partial argon atmosphere. The sealed quartz ampoule was heated to and soaked at 1323 K, then slowly cooled down to 1123 K. Finally, the ampoule was decanted with a centrifuge. X-ray diffraction (XRD) of a single crystal were performed using a Bruker D8 X-ray machine with  $\text{Cu } K_\alpha$  radiation. Electrical transport measurements were carried out by using Quantum Design PPMS-14T. The longitudinal and Hall electrical resistivity were performed using a four-probe method on crystals with size of  $1 \times 0.7 \times 0.2 \text{ mm}^3$ . The current flows in the  $ab$  plane and the magnetic field is perpendicular to current direction. The Hall resistivity was obtained by the difference of transverse resistance measured at the positive and negative fields in order to effectively get rid of the longitudinal resistivity contribution due to voltage probe misalignment, i.e.,  $\rho_{xy}(\mu_0 H) = [\rho(+\mu_0 H) - \rho(-\mu_0 H)]/2$ . The first-principles electronic structure calculations were implemented with the projector augmented wave method [15] as implemented in the VASP package [16]. For the exchange-correlation potential, the generalized gradient approximation of Perdew-Burke-Ernzerhof type [17] was used. The kinetic energy cutoff of the plane wave basis was set to be 300 eV. For the Brillouin zone sampling, a  $10 \times 10 \times 10$  k-point mesh was employed. The spin-orbital-coupling effect was included in the calculations of electronic properties. The maximally localized Wannier functions [18, 19] was used to calculate the Fermi surfaces (FSs).

## 3. Results and discussion

$\text{LaBi}$  has a NaCl-type centrosymmetric structure with the symmorphic space group Fm-3m. The Wyckoff position of La and Bi are  $4a$  (0, 0, 0) and  $4b$  (1/2, 1/2, 1/2), respectively. The XRD pattern of a  $\text{LaBi}$  single crystal indicates that the surface of crystal is the (1 0 0) plane (figure 1(a)). The cubic-shape  $\text{LaBi}$  crystals (inset of figure 1(a)) is consistent with the single crystal XRD pattern and its crystallographic symmetry. As shown in figure 1(b), the zero-field resistivity  $\rho_{xx}(T, 0)$  of  $\text{LaBi}$  single crystal exhibits metallic behavior, similar to that in  $\text{LaSb}$  [11]. The residual resistance ratio [ $\text{RRR} \equiv R(300 \text{ K})/R(2 \text{ K}) = 204$ ] indicates the high quality of sample. The linear temperature dependence of  $\rho_{xx}(T, 0)$  at high temperatures suggests the electron-phonon ( $e$ - $ph$ ) scattering is the dominant scattering mechanism. In contrast, the  $\rho_{xx}(T, 0)$  at low-temperature region ( $2 \text{ K} \leq T \leq 20 \text{ K}$ ) can be well fitted by using the formula  $\rho_{xx}(T, 0) = \rho_0 + AT^n$  with  $\rho_0 = 0.1765(3) \mu\Omega \text{ cm}$ ,  $A = 2.528(4) \times 10^{-5} \mu\Omega \text{ cm K}^{-3}$  and  $n = 2.99(1)$  (inset of figure 1(b)). The value of  $\rho_0$  is larger than that in  $\text{LaSb}$  ( $\rho_0 = 0.08 \mu\Omega \text{ cm}$ ) but the  $n$  is smaller ( $n = 4$  for  $\text{LaSb}$ ) [11]. The values of  $n$  for both systems

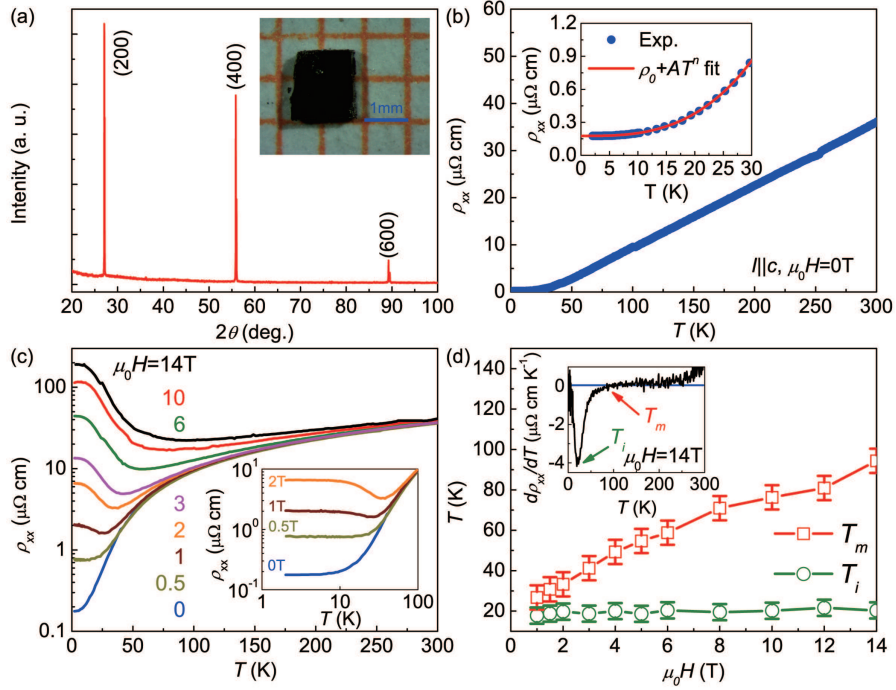


**Figure 1.** (a) XRD of a LaBi single crystal at 300 K. Inset: photo of typical LaBi single crystal. (b) Temperature dependence of  $\rho_{xx}(T, 0)$  for  $I \parallel c$ . Insets: enlarged parts of  $\rho_{xx}(T, 0)$  below 20 K. The solid line is the fit using the formula  $\rho_{xx}(T, 0) = \rho_0 + AT^n$ . (c) Temperature dependence of  $\rho_{xx}(T, \mu_0 H)$  at various fields. Inset: enlarged parts of  $\rho_{xx}(T, \mu_0 H)$  at low-temperature region under low fields. (d) Field dependence of  $T_m$  and  $T_i$ , corresponding to the sign change and the minimum in the  $d\rho_{xx}(T, \mu_0 H)/dT$  curves, respectively. Inset:  $d\rho_{xx}(T, \mu_0 H)/dT$  vs.  $T$  at 14 T. The positions of  $T_m$  and  $T_i$  are marked by arrows.

distinctly different from  $n = 2$  when  $e$ - $e$  scattering is dominant, such as in  $\text{WTe}_2$  [20]. These values are also smaller than  $n = 5$  for the conventional  $e$ - $ph$  scattering process according to the Bloch-Grüneisen theory [21]. It suggests that the interband  $s$ - $d$   $e$ - $ph$  scattering, rather than the intraband  $s$ - $s$   $e$ - $ph$  scattering should be dominant at low temperature [21]. Similar behavior has been observed in yttrium metal as well as in other transition metal carbide [22, 23].

Figure 1(c) shows the  $\rho_{xx}(T, \mu_0 H)$  at various fields up to 14 T. When the field is low, the  $\rho_{xx}(T, \mu_0 H)$  still exhibits metallic behavior in the whole temperature region, similar to the  $\rho_{xx}(T, 0)$ . Once the field is beyond the critical field  $\mu_0 H_c$  ( $\sim 0.5$  T) (inset of figure 1(c)), the  $\rho_{xx}(T, \mu_0 H)$  curves show a minimum at field-dependent "turn-on" temperatures  $T_m(\mu_0 H)$ , i.e., the  $\rho_{xx}(T, \mu_0 H)$  increases significantly with decreasing temperature. This behavior has been observed not only in LaSb but also in other XMR materials, such as  $\text{WTe}_2$  and NbP [6, 10, 11]. Correspondingly, when  $\mu_0 H > \mu_0 H_c$ , the  $d\rho_{xx}(T, \mu_0 H)/dT$  is positive at  $T > T_m$  and changes the sign at  $T < T_m$  (inset of figure 1(d)). When the field increases, the  $T_m$  shifts to higher temperature, but another characteristic temperature  $T_i$  related to the inflection point of  $\rho_{xx}(T, \mu_0 H)$  seems insensitive to the field (figure 1(d)). Both characteristic temperatures merge together

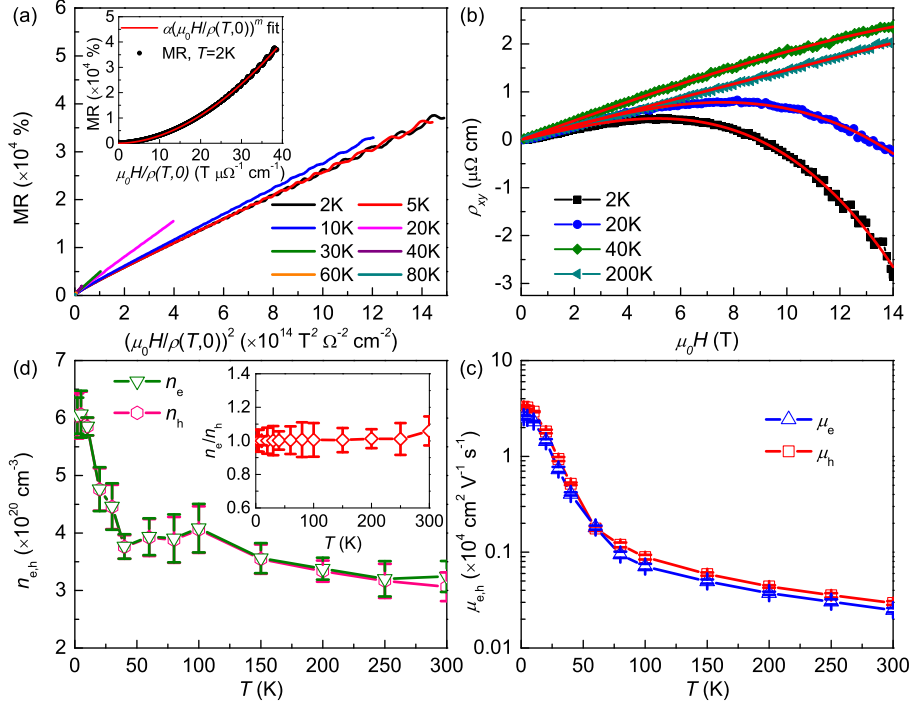


**Figure 2.** (a) MR vs.  $[\mu_0 H / \rho_{xx}(T, 0)]^2$  at  $T \leq 80$  K. Inset: MR at 2 K. The solid line is the fit using  $\alpha[\mu_0 H / \rho_{xx}(T, 0)]^m$ . (b) Field dependence of  $\rho_{xy}(T, \mu_0 H)$  at various temperatures. The red solid lines are the fits using the two-band model. (c) Temperature dependence of fitted  $n_{e,h}(T)$ . Inset: the ratio of  $n_e/n_h$  a function of  $T$ . (d) Temperature dependence of fitted  $\mu_{e,h}(T)$ .

when  $\mu_0 H \sim \mu_0 H_c$ . Moreover, there is a plateau in  $\rho_{xx}(T, \mu_0 H)$  curves following the upturn behavior at low temperatures and high fields. Similar behaviors have been observed in LaSb [11].

LaBi exhibits rather large MR ( $= (\rho_{xx}(T, \mu_0 H) - \rho_{xx}(T, 0)) / \rho_{xx}(T, 0) = \Delta\rho_{xx}(T, \mu_0 H) / \rho_{xx}(T, 0)$ ) at low temperature and the MR at 2 K is  $3.8 \times 10^4 \%$  under 14 T (figure 2(a)). Although the MR at 9 T ( $\sim 1.6 \times 10^4 \%$ ) is one order of magnitude smaller than that in LaSb, it is still comparable with the MRs in other XMR materials [5, 8, 11]. The MR of LaBi does not saturate up to 14 T and when the field is larger than about 5 T, the Shubnikov-de Haas (SdH) quantum oscillations (QOs) appears at low temperature (figure 2(a)). When  $T \leq 10$  K, the MR decreases gradually with increasing temperature, but drops quickly at higher temperatures. According to the Kohler's rule [20, 21],  $\text{MR} = \alpha(\mu_0 H / \rho_{xx}(T, 0))^m$ , if the carrier concentration of sample is weakly temperature dependent, the MR measured at various temperatures can be scaled into a single curve. But the scaled MR curves do not fall into one curve for LaBi (figure 2(a)), obviously deviating from the Kohler's rule. This violation strongly suggests that the carrier concentrations and/or the mobility ratio of hole to electron change significantly with temperature [20, 24]. The fit of MR curve at 2 K gives  $\alpha = 0.411(4) (\mu\Omega \text{cm T}^{-1})^{1.866}$  and  $m = 1.866(2)$  (inset of figure 2(a)), close to the typically quadratic field dependence of the MR in the multiband metals.

Hall resistivity  $\rho_{xy}(T, \mu_0 H)$  of LaBi (figure 2(b)) is positive at high temperature with nearly linear field dependence and when lowering temperature, the  $\rho_{xy}(T, \mu_0 H)$  exhibits nonlinear behavior and becomes negative at high field. Moreover, the QOs are clearly seen at 2 K, consistent with the MR results. The  $\rho_{xy}(T, \mu_0 H)$  can be fitted using the two-band model [20, 21],

$$\rho_{xy} = \frac{\mu_0 H}{e} \frac{(n_h \mu_h^2 - n_e \mu_e^2) + (n_h - n_e)(\mu_e \mu_h)^2 (\mu_0 H)^2}{(n_h \mu_h + n_e \mu_e)^2 + (n_h - n_e)^2 (\mu_e \mu_h)^2 (\mu_0 H)^2} \quad (1)$$

where  $n_{e,h}$  and  $\mu_{e,h}$  are the carrier concentrations and mobilities of electron and hole, respectively. The fits are quiet well (solid lines in figure 2(b)) and the obtained  $n_{e,h}(T)$  and  $\mu_{e,h}(T)$  as a function of temperature are shown in figure 2(c) and (d). At  $T > 40$  K, the  $n_{e,h}(T)$  is weakly temperature dependent. When lowering temperature, the  $n_{e,h}(T)$  increase gradually at the beginning and then become saturated. The estimated carrier concentration at 2 K is  $6.0(4)$  and  $6.0(3) \times 10^{20} \text{ cm}^{-3}$  for  $n_e$  and  $n_h$ , respectively. Such small  $n_{e,h}$  with two types of carriers confirms the semimetallicity of LaBi. More importantly, the ratio of  $n_e/n_h$  is almost one with slightly larger  $n_e$  than  $n_h$  in the whole temperature range, strongly suggesting that the carriers in LaBi is nearly compensated. On the other hand, the  $\mu_{e,h}(T)$  monotonically increases with decreasing temperature with a larger slope between 10 - 40 K and becomes rather high at low temperature ( $2.6(1)$  and  $3.3(1) \times 10^4 \text{ cm}^2 \text{ V}^{-1} \text{ s}^{-1}$  for  $\mu_e$  and  $\mu_h$  at 2 K, respectively). Strong temperature dependence of  $n_{e,h}(T)$  and  $\mu_{e,h}(T)$  between 10 - 40 K possibly causes the obvious violation of Kohler's rule in this temperature range (figure 2(a)).

The QOs as a function of  $1/(\mu_0 H)$  at low temperatures are shown in figure 3(a). The amplitudes of QOs decrease with increasing temperature or decreasing field. The fast Fourier transform (FFT) spectra of the QOs reveals two principal frequencies  $F_\alpha = 276 \text{ T}$  with its second harmonic frequency  $F_{2\alpha} = 555 \text{ T}$  and  $F_\beta = 610.5 \text{ T}$  (figure 3(b)). All of these frequencies are higher than those in LaSb [11], indicating LaBi has larger FSs than LaSb, agreeing with the results of Hall measurement [11]. According to the Onsager relation  $F = (\hbar/2\pi e)A_F$ , where  $A_F$  is the extremal cross section of FS. The determined  $A_F$  is 0.027 and  $0.058 \text{ \AA}^{-2}$  for  $\alpha$  and  $\beta$  bands, respectively, consistent with previous results [25]. These  $A_F$ s are very small, taking only  $\sim 2.9$  and  $6.4 \%$  of the whole area of Brillouin zone in the  $k_x - k_y$  plane providing the lattice parameter  $a = 6.58 \text{ \AA}$ . Because the FS of  $\beta$  band is almost spherical [25], and there is only one  $\beta$  FS in one Brillouin zone according to the band structure calculation shown below, the estimated carrier concentration for  $\beta$  band  $n_h^\beta$  is  $0.85 \times 10^{20} \text{ cm}^{-3}$ . The effective mass  $m^*$  can be extracted from the temperature dependence of the amplitude of FFT peak using the Lifshitz-Kosevich (LK) formula [26],

$$\Delta\rho_{xx} \propto \frac{X}{\sinh X} e^{-2\pi^2 k_B T_D / \hbar \omega_c} \cos 2\pi(F/(\mu_0 H) + 1/2 - \beta + \delta) \quad (2)$$

where  $X = 2\pi^2 k_B T / \hbar \omega_c = 14.69 m^* / \mu_0 H_{avg}$  with  $\hbar \omega_c$  being the cyclotron frequency and  $\mu_0 H_{avg} = [(14 - 5.44)/2 = 9.72 \text{ T}]$  being the average value of the field window used for the FFT spectra of QOs [27].  $T_D^\alpha$  is the Dingle temperature,  $\beta$  is the Berry's phase,



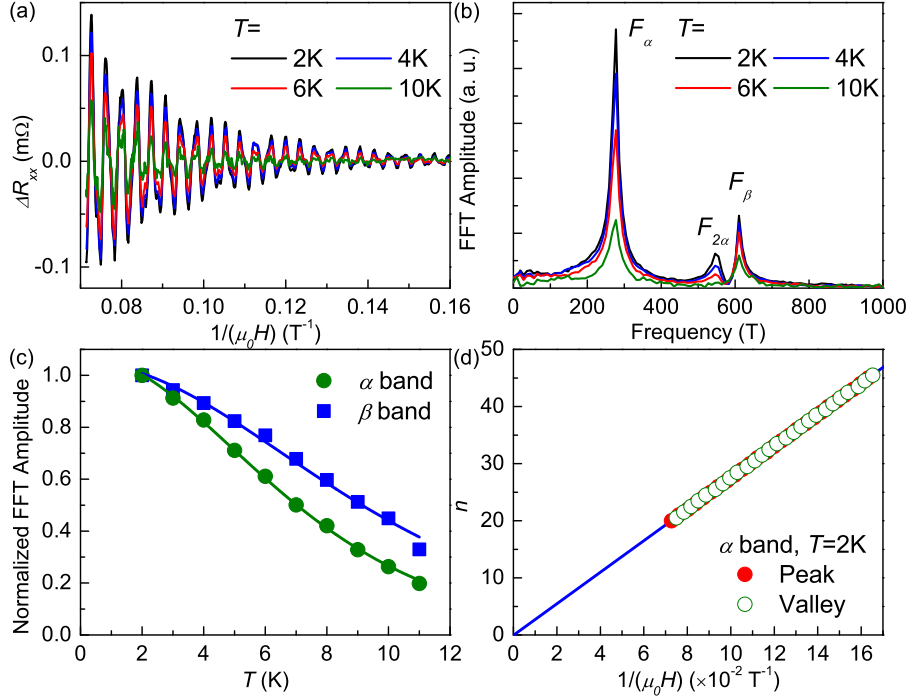


**Figure 3.** (a) SdH QOs  $\Delta R_{xx} = R_{xx} - \langle R_{xx} \rangle$  as a function of  $1/(\mu_0 H)$  at various temperatures. (b) FFT spectra of the QOs at various temperatures. (c) The temperature dependence of FFT amplitudes of  $\alpha$  and  $\beta$  peaks, normalized by their 2 K values. The solid lines are the fits using the LK formula, giving the effective masses. (d) The Landau level indices  $n$  as a function of  $1/(\mu_0 H)$  for the  $\alpha$  band. The solid and empty symbols correspond to the positions of peaks and valleys in  $\Delta R_{xx}$  curve at 2 K, respectively. The solid line represents the linear fit of data.

and  $\delta$  is a phase shift determined by the dimensionality ( $\delta = \pm 1/8$  for the 3D system) [26, 28, 29]. The fitted  $m^*$  of  $\alpha$  and  $\beta$  band is 0.217(1) and 0.164(3)  $m_e$ , respectively, where  $m_e$  is the bare electron mass (figure 3(c)). The fitted  $T_D$  from the decaying amplitude of QOs with field at 2 K [26] gives 9(1) K for the  $\alpha$  band, corresponding to the quantum lifetime  $\tau_Q^\alpha = \frac{\hbar}{2\pi k_B T_D^\alpha} = 1.2(2) \times 10^{-13}$  s. According to eq. (2), the Landau Level (LL) index  $n$  is related to the QO frequency  $F$  by the Lifshitz-Onsager quantization rule  $F/(\mu_0 H) = n + 1/2 - \beta + \delta$  [26, 28, 29]. The peaks and valleys of the  $\Delta R_{xx}$  at 2 K are assigned as integer ( $n$ ) and half integer ( $n + 1/2$ ) LL indices, respectively. Linear fit of  $n$  vs.  $1/(\mu_0 H)$  yields  $F = 275.9(4)$  T and  $1/2 - \beta + \delta = -0.05(5)$  (figure 3(d)). For normal metals with trivial parabolic dispersion relation, the Berry's phase  $2\pi\beta = 0$ . For Dirac systems with linear dispersion, there should be a nontrivial  $\pi$  Berry's phase ( $\beta = 1/2$ ), as observed in 2D graphene and 3D Dirac semimetal Cd<sub>3</sub>As<sub>2</sub> [30, 31]. The obtained  $\beta = 0.55(5) + 2\pi\delta$  indicates a possible nontrivial  $\pi$  Berry's phase for the  $\alpha$  band of LaBi. It should be noted that because the lowest LL obtained at present is  $n = 7$  which is far from the quantum limit, there might be a relatively large uncertainty when determining the intercept. This nontrivial  $\pi$  Berry's phase needs to be further confirmed by the measurement at much higher field in order to be closer the quantum limit.

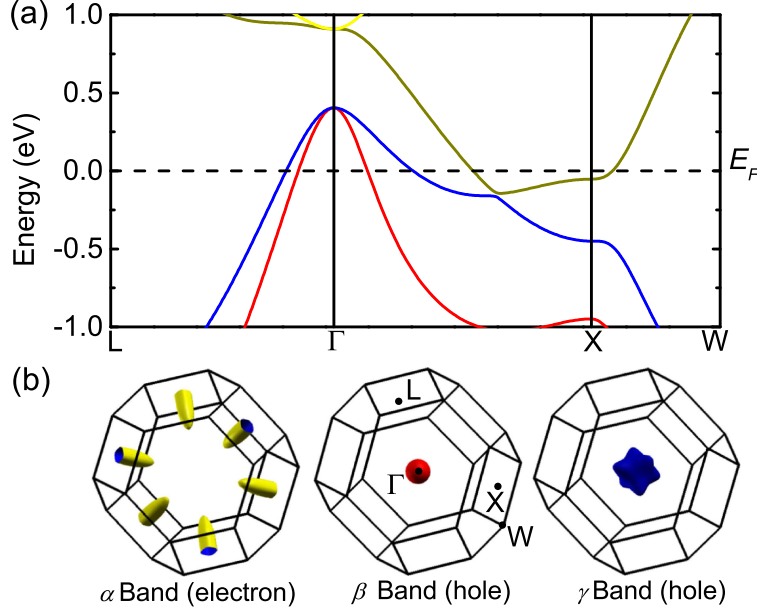


**Figure 4.** (a) Band structure and (b) FSs of LaBi calculated with the SOC effect. The dashed line denotes the position of  $E_F$ . There are three FSs at  $E_F$ , including two hole-type FSs around  $\Gamma$  point and one electron-type FS around  $X$  point.

Similar to LaSb [11, 32], theoretical calculation indicates that there are three bands crossing  $E_F$  in LaBi (figure 4(a)), consistent with QOs results and previous calculations [25]. The electron-type band ( $\alpha$  band) is located at  $X$  point with the ellipsoidal FS with longest principle axis along  $\Gamma - X$  line; Two hole-type bands ( $\beta$  and  $\gamma$  bands) are centered at  $\Gamma$  point. One has a nearly spherical FS and another one has a FS stretched in the  $< 100 >$  directions (figure 4(b)). The calculated  $n_{e,h}$  are  $3.52$ ,  $0.72$ , and  $2.88 \times 10^{20} \text{ cm}^{-3}$  for the  $\alpha$ ,  $\beta$ , and  $\gamma$  bands, strongly indicating that LaBi is a nearly compensated SM ( $\lambda = n_e/n_h = 0.98$ ).

Because LaSb and LaBi seem nearly compensated SMs, similar to  $\text{WTe}_2$ , we develop the model proposed to explain the magnetotransport properties of  $\text{WTe}_2$  [20] to analysis the common features in (nearly) compensated SMs. According to the two-band model [20, 21], the MR can be expressed

$$\text{MR} = \frac{n_e \mu_e n_h \mu_h (\mu_e + \mu_h)^2 (\mu_0 H)^2}{(n_e \mu_e + n_h \mu_h)^2 + (n_e - n_h)^2 (\mu_e \mu_h)^2 (\mu_0 H)^2} \quad (3)$$

for the compensated SMs ( $n_e = n_h = n_c$ ), we have  $\text{MR} = \mu_e \mu_h (\mu_0 H)^2$ . Thus, the large MR is directly related to the high mobilities of materials. If assuming  $\rho_{xx}(T, 0) = \rho_0 + AT^n$ , we get

$$\rho_{xx}(T, \mu_0 H) = \rho_0 + AT^n + \alpha (\mu_0 H)^2 / (\rho_0 + AT^n) \quad (4)$$

where  $\alpha = \kappa [n_c e (1 + \kappa)]^{-2}$  and  $\kappa = \mu_h / \mu_e$  [20]. Therefore, we will return to the Kohler's rule with  $m = 2$ . More importantly, according to eq. (4), there is a minimum in  $\rho_{xx}(T, \mu_0 H)$  curve when  $\mu_0 H > \mu_0 H_c (= \rho_0 / \alpha^{1/2})$  [20], i.e., field-induced resistivity upturn. The simulated  $\rho_{xx}(T, \mu_0 H)$  curves with  $\mu_0 H_c = 0.28 \text{ T}$  clearly reflect



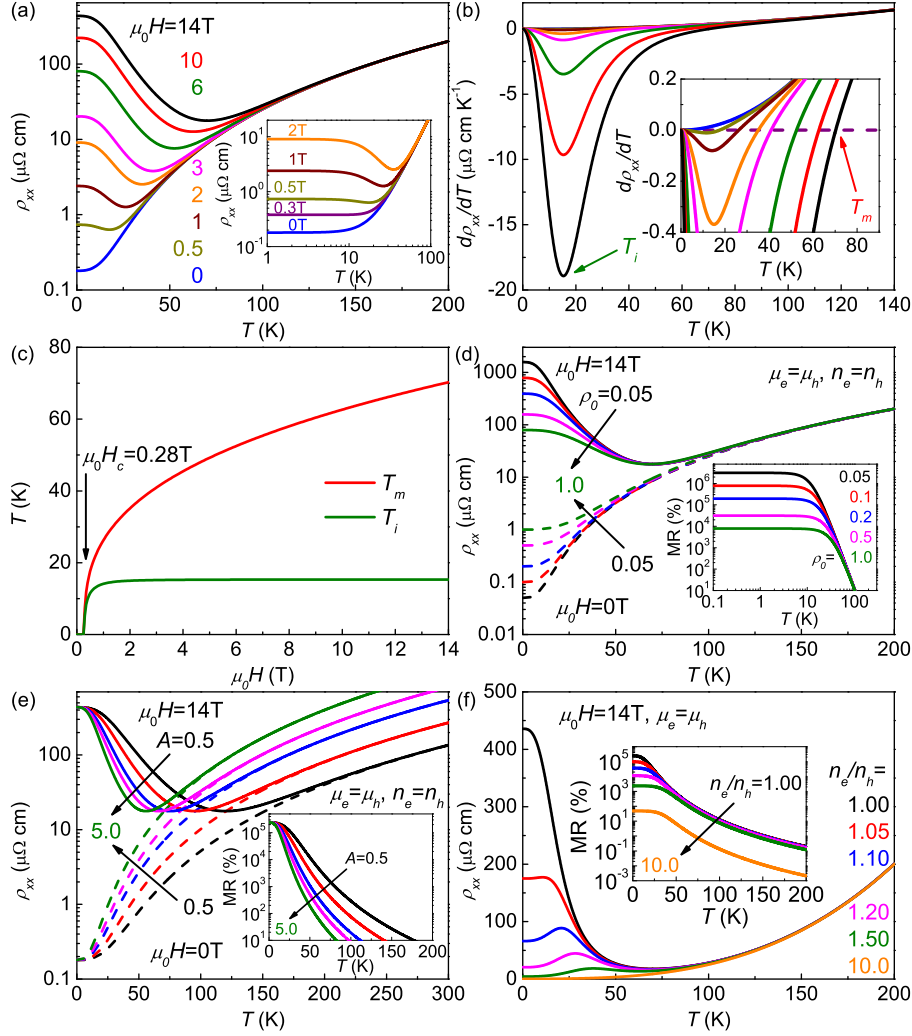


**Figure 5.** Simulation of longitudinal resistivity with  $\rho_0 = 0.18 \mu\Omega \text{ cm}$ ,  $A = 2.5 \times 10^{-5} \mu\Omega \text{ cm K}^{-3}$ ,  $n = 3$ , and  $\alpha = 0.4 (\mu\Omega \text{ cm T}^{-1})^2$ . (a)  $\rho_{xx}(T, \mu_0 H)$  vs.  $T$  at various fields with  $\mu_0 H_c = 0.28 \text{ T}$ . Inset: simulated  $\rho_{xx}(T, \mu_0 H)$  vs.  $T$  when the fields are near  $\mu_0 H_c$ . (b) Corresponding  $d\rho_{xx}(T, \mu_0 H)/dT$  as a function of  $T$  at various fields. Inset displays the changes of  $T_m$  with field. The color code is same as in (a). (c) Field dependence of derived  $T_m$  and  $T_i$ . (d)  $\rho_{xx}(T, \mu_0 H)$  vs.  $T$  at  $\mu_0 H = 0$  (dashed lines) and  $14 \text{ T}$  (solid lines) with  $\rho_0 = 0.05, 0.1, 0.2, 0.5$ , and  $1.0 \mu\Omega \text{ cm}$ . (e)  $\rho_{xx}(T, \mu_0 H)$  vs.  $T$  at  $\mu_0 H = 0$  (dashed lines) and  $14 \text{ T}$  (solid lines) with  $A = 0.5, 1, 2, 3$ , and  $5 \times 10^{-5} \mu\Omega \text{ cm K}^{-3}$ . (f)  $\rho_{xx}(T, \mu_0 H)$  vs.  $T$  at various  $n_e/n_h$  with  $\mu_0 H = 14 \text{ T}$ . Insets of (d)-(f): temperature dependence of corresponding MR at  $\mu_0 H = 14 \text{ T}$ .

this behavior and fairly well reproduce the experimental results (figure 5(a)). Firstly, the  $\rho_{xx}(0, \mu_0 H)$  is not infinity but  $\rho_0 + \alpha(\mu_0 H)^2/\rho_0$ , i.e., there is a resistivity plateau at low temperature with the absolute value increasing at higher field. Secondly, the simulated field dependence of  $T_m$  and  $T_i$  well reflect the features observed in LaSb [11] and LaBi (figure 5(b) and (c)). The  $T_m$  is proportional to  $(\mu_0 H - \mu_0 H_c)^{1/n}$  (here,  $n = 3$  for LaBi) and the  $T_i$  saturates quickly when field is large. Noted that both  $T_i(\mu_0 H_c)$  and  $T_m(\mu_0 H_c)$  become zero but these trend are not observed experimentally, possibly because the initial slope of  $T_i(\mu_0 H_c)$  and  $T_m(\mu_0 H_c)$  are very large and the  $\rho_{xx}(T, \mu_0 H)$

is too flat to extract accurate  $T_i$  and  $T_m$  when  $\mu_0 H$  is close to  $\mu_0 H_c$ .

Thirdly, if assuming  $\mu_e = \mu_h = \mu$  and temperature-independent  $n_e = n_h = n_c$ , it has  $\rho = \sigma^{-1} = (n_e e \mu_e + n_h e \mu_h)^{-1} = (2n_c e \mu)^{-1} = \rho_0 + AT^n$ , and thus when  $\mu$  increases, it corresponds to the decrease of either  $\rho_0$  and/or  $A$ . Figure 5(d) shows the influence of  $\rho_0$  on magnetotransport behavior. It can be seen that with smaller  $\rho_0$ , the upturn behavior becomes more obvious. Moreover because the increase of  $\rho_{xx}(T, \mu_0 H)$  at high field is accompanied by the decrease of  $\rho_{xx}(T, 0)$ , the MR at low temperature region is remarkably influenced by the  $\rho_0$  (inset of figure 5(d)). The small  $\rho_0$ , partly originating from the large  $\mu$ , will lead to much obvious MR. It is consistent with the results in terms of eq. (3) under compensation condition. On the other hand, if  $\rho_0$  is fixed, i.e.,  $\mu(0) = \text{constant}$ , the smaller  $A$  leads to the weaker decay of  $\mu(T)$  with increasing temperature, and thus the upturn behavior appears higher temperature region and becomes more obvious (figure 5(e)). Correspondingly, the MR at same temperature and field becomes large with smaller  $A$  (inset of figure 5(e)). Overall, the increase of  $\mu$  is in favor of field-induced upturn behavior and large MR.

Finally, we examine the influence of the mobilities on the uncompensation between electron and hole on the field-induced upturn behavior. If assuming  $\mu_e = \mu_h$ , we get

$$\rho_{xx}(T, \mu_0 H) = \rho_0 + AT^n + \frac{4\lambda(\rho_0 + AT^n)(\mu_0 H)^2}{\beta^2(\rho_0 + AT^n)^2(\lambda + 1)^4 + (\lambda - 1)^2(\mu_0 H)^2} \quad (5)$$

where  $\beta = \frac{1}{2\sqrt{\alpha}}$ . When  $\lambda (= n_e/n_h)$  increases, although the  $\rho_{xx}(0, \mu_0 H)$  decreases gradually, there is still a remarkable resistivity upturn with a plateau even extending to the higher temperature (figure 5(d)). It indicates that the field-induced resistivity upturn is robust to the imbalance between  $n_e$  and  $n_h$ . Surprisingly, a reentrant metallic behavior is observed with further increasing  $\lambda$ . It is because the second item of the denominator in eq. (5), originating from the uncompensated carriers, weakens the effect of field on  $\rho_{xx}(T, \mu_0 H)$  at low temperature. Correspondingly, the MR also decreases with increasing  $\lambda$  (inset of figure 5(f)). In the extreme case that the  $n_e$  and  $n_h$  are severely imbalanced, the upturn behavior even disappears (Fig. 5(d)) since the system will become a (nearly) single-band system where the MR is very small, i.e., the field does not have effect on  $\rho_{xx}(T, \mu_0 H)$ . We have to mention that above analysis is valid when  $n \geq 2$ .

In order to further confirm the validity of above analysis, the calculated  $\rho_{xx}(0, \mu_0 H)$  using the temperature dependent  $n_{e,h}$  and  $\mu_{e,h}$  derived from the two-band model analysis is plotted together with the measured  $\rho_{xx}(0, \mu_0 H)$  (figure 6). It can be seen that both of results are consistent with each other very well and similar analysis was carried out in classic semimetallic bismuth and graphite [33]. It strongly implies that the origin of field-induced properties in LaBi, similar to other semimetals with compensated carriers, can be well understood in the framework of multiband model. Noted that recently discovered TaSb<sub>2</sub> [34] seems to exhibit similar behaviors as in LaPn. Thus, it would be interest to examine if our analysis will apply to this system.

Except the electron-hole compensation mechanism, the magnetic field lifting of topologically protected backscattering in topological SMs could also lead to XMR [8].

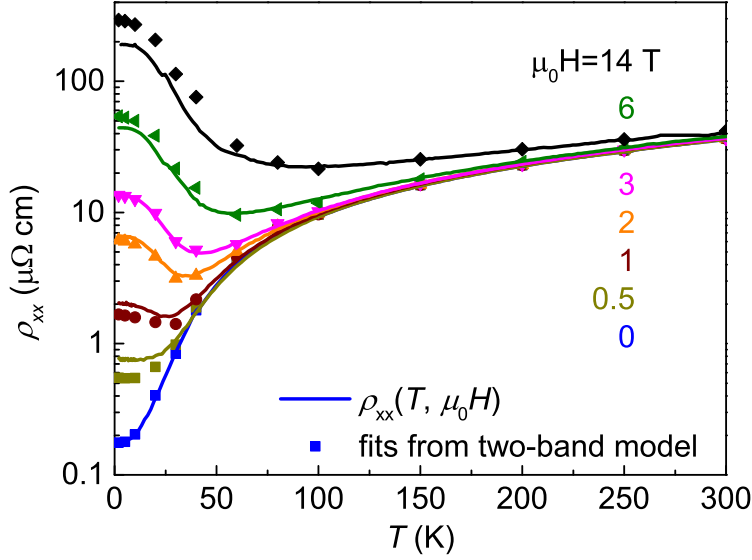


**Figure 6.** Temperature dependence of  $\rho_{xx}(T, \mu_0 H)$  at various fields (solid lines). The scatters are calculated using the temperature dependent  $n_{e,h}$  and  $\mu_{e,h}$  derived from the two-band model analysis.

In these systems, the backscattering is strongly suppressed at zero field, resulting in a transport lifetime  $\tau_{tr}$  much longer than the quantum lifetime  $\tau_Q$ . We check this possible mechanism of XMR in LaBi. The  $\tau_{tr} = m^* \mu_{e,h} / e$  is  $2.59(6) \times 10^{-12}$  s and the ratio  $\tau_{tr} / \tau_Q^\alpha$  ( $\sim 22$ ) is much smaller than those in Dirac SM  $\text{Cd}_3\text{As}_2$  ( $\sim 10^4$ ) and Weyl SM  $\text{NbAs}$  ( $\sim 10^3$ ) [7, 8], implying that there may be little topological protection for the  $\alpha$  band of LaBi.

#### 4. Conclusion

In summary, LaBi exhibits the XMR and field-induced resistivity upturn, similar to isostructural LaSb. Based on the two-band model, these behaviors can be well understood and the electron-hole compensation mechanism seems dominant in LaBi. The key conditions leading to the XMR and field-induced properties in SMs are *significantly high*  $\mu_{e,h}$ , *extremely small*  $\rho_0$ , and *rather low*  $n_{e,h}$  *satisfying the compensation condition*. Because theoretical calculation suggests that LaP and LaAs have smaller overlap between electron- and hole-type bands with lower  $n_{e,h}$  than LaSb [32], it is worth inspecting if they will exhibit even larger MR. Systematical studies on  $\text{LaPn}$  family with simple electron structure will not only deepen our understanding on XMR phenomenon but also shed light on exploring novel XMR materials with prominent properties for potential applications.

#### Acknowledgments

This work was supported by the Ministry of Science and Technology of China (973 Project: 2012CB921701), the Fundamental Research Funds for the Central Universities,

and the Research Funds of Renmin University of China (14XNLQ03 and 15XNLF06), and the National Nature Science Foundation of China (Grant No. 11574394). Computational resources have been provided by the Physical Laboratory of High Performance Computing at RUC.

† These authors contributed equally to this work.

## Reference

- [1] Daughton J M, Magn J 1999 *Magn. Mater.* **192** 334
- [2] Baibich M N, Broto J M, Fert A, Nguyen Van Dau F, Petroff F, Etienne F, Creuzet G, Friederich A and Chazelas J 1988 *Phys. Rev. Lett.* **61** 2472
- [3] Ramirez A P, Cava R J and Krajewski J 1997 *Nature*. **386** 156
- [4] Jin S, McCormack M, Tiefel T H and Ramesh R 1994 *J. Appl. Phys.* **76** 6929
- [5] Huang X C, Zhao L X, Long Y J, Wang P P, Chen D, Yang Z H, Liang H, Xue M Q, Weng H M, Fang Z, Dai X and Chen G F 2015 *Phys. Rev. X*. **5** 031023
- [6] Shekhar C, Nayak A K, Sun Y, Schmidt M, Nicklas M, Leermakers I, Zeitler U, Liu Z K, Chen Y L, Schnelle W, Grin J, Felser C and Yan B H 2015 *Nature. Phys.* **11** 645
- [7] Luo Y, Ghimire N J, Wartenbe M, Choi H, Neupane M, McDonald R D, Bauer E D, Zhu J, Thompson J D and Ronning F 2015 *Phys. Rev. B* **92** 205134
- [8] Liang T, Gibson Q, Ali Mazhar N, Liu M H, Cava R J and Ong N P 2015 *Nature. Mater.* **14** 280
- [9] Wang K, Graf D, Li L, Wang L and Petrovic C 2014 *Sci. Rep.* **4** 7328
- [10] Mazhar N A, Jun X, Flynn S, Jing T, Gibson Q D, Schoop L M, Tian L, Haldolaarachchige N, Hirschberger M, Ong N P and Cava R J 2014 *Nature*. **514** 205
- [11] Tafti F F, Gibson Q D, Kushwaha S K, Haldolaarachchige N and Cava R J 2016 *Nat. Phys.* **12** 272
- [12] Kasuya T, Sera M and Suzuki T 1993 *J. Phys. Soc. Jpn.* **62** 2561
- [13] Kasuya T, Sera M, Okayama Y and Haga Y 1996 *J. Phys. Soc. Jpn.* **65** 160
- [14] Zeng L K, Lou R, Wu, D S, Guo P J, Kong L Y, Zhong Y G, Ma J Z, Fu B B, Richard P, P. Wang, G. T. Liu G T, Lu L, Sun S S, Wang Q, Wang L, Shi Y-G, Lei H C, Liu, K, Wang S C, Qian T, Luo J L, and Ding H 2016 *arXiv*: 1604.08142
- [15] Blöchl P E 1994 *Phys. Rev. B* **50** 17953 ; Kresse G and Joubert D 1999 *Phys. Rev. B* **59** 1758
- [16] Kresse G and Hafner J 1993 *Phys. Rev. B* **47** 558(R) ; Kresse G and Furthmüller J 1996 *Comp. Mater. Sci.* **6** 15 ; Kresse G and Furthmüller J 1996 *Phys. Rev. B* **54** 11169
- [17] Perdew J P, Burke K and Ernzerhof M 1996 *Phys. Rev. Lett.* **77** 3865
- [18] Marzari N and Vanderbilt D 1997 *Phys. Rev. B* **56** 12847
- [19] Souza I, Marzari N and Vanderbilt D 2001 *Phys. Rev. B* **65** 035109
- [20] Wang Y L, Thoutam L R, Xiao Z L, Hu J, Das S, Mao Z Q, Wei J, Divan R, Luican-Mayer A, Crabtree G W and Kwok W K 2015 *Phys. Rev. B* **92** 180402(R)
- [21] Ziman J M 2001 *Electrons and Phonons, Classics Series* (Oxford University Press, New York)
- [22] Araj S and Colvin R V 1962 *J. Less-Common. Met.* **4** 572
- [23] Zhang X, Xiao Z, Lei H C, Toda Y, Matsuishi S, Kamiya T, Ueda S and Hosono H 2014 *Chem. Mater.* **26** 6638
- [24] Zhao Y, Liu H, Yan J, An W, Liu J, Zhang X, Wang H, Liu Y, Jiang H, Li Q, Wang Y, Li X Z, Mandrus D, Xie X C, Pan M and Wang J 2015 *Phys. Rev. B* **92** 041104(R)
- [25] Hasegawa A, 1985 *J. Phys. Soc. Jpn.* **54** 677
- [26] Shoenberg D 1984 *Magnetic Oscillations in Metals* (Cambridge University Press, Cambridge, England)
- [27] Rhodes D, Das S, Zhang Q R, Zeng B, Pradhan N R, Kikugawa N, Manousakis E, and Balicas L 2015 *Phys. Rev. B* **92** 125152
- [28] Mikitik G P and Sharlai Yu V 1999 *Phys. Rev. Lett.* **82** 2147

- [29] Luk'yanchuk I A and Kopelevich Y 2004 *Phys. Rev. Lett.* **93** 166402
- [30] Novoselov K S, Geim A K, Morozov S V, Jiang D, Katsnelson M I, Grigorieva I V, Dubonos S V, and Firsov A A, 2005 *Nature* **438**, 197
- [31] He L P, Hong X C, Dong J K, Pan J, Zhang Z, Zhang J, and Li S Y 2014 *Phys. Rev. Lett.* **113** 246402
- [32] Zeng M G, Fang C, Chang G Q, Chen Y A, Hsieh T, Bansil A, Lin H and Fu L 2015 *arXiv*: 1504.03492
- [33] Du X, Tsai S W, Maslov D L, and Hebard A F 2005 *Phys. Rev. Lett.* **94** 166601
- [34] Li Y, Li L, Wang J, Wang T, Xu X, Xi C, Cao C and Dai J 2016 *arXiv*: 1601.02062